

Use and Accuracy of Numerical Weather Predictions to Support EM Wave Propagation Experiments

Laurent Quibus, Lorenzo Luini, Carlo Riva, and Danielle Vanhoenacker-Janvier

Abstract—In order to keep up with the demand for new services, future satellite-to-ground communications will operate at higher frequencies, notably in the 20-50 GHz bands. Consequently, new challenges arise for system designers as the attenuation of the signal crossing the troposphere increases with frequency. Propagation experiments, such as the on-going Alphasat campaign, provide direct measurements of the attenuation. However, other data sources, such as collocated radiometers, are needed to recover the attenuation in nonrainy conditions. This work uses the Weather Research and Forecasting (WRF) software and investigates Numerical Weather Prediction (NWP) models as an alternative source of nonrainy attenuation time series. Four months of measured Alphasat and radiometric signals collected at Spino d’Adda serve as the reference to assess the accuracy of NWP-derived attenuation. The best agreement between the NWP-derived and the radiometric nonrainy attenuations is achieved with the Tiedtke cumulus scheme. Considering the limits in accuracy inherent to the propagation and radiometric data, the resulting total attenuation statistics are acceptable. The results are expected to improve further with NWP simulation domains closer to the state-of-the-art.

Index Terms—Alphasat, microwave radiometry, nonrainy attenuation, Numerical Weather Prediction (NWP), radiowave propagation, Weather Research and Forecasting (WRF).

I. INTRODUCTION

THE electromagnetic (EM) wave propagation community recognizes the interest for Earth-Space links operating at higher frequencies. Firstly, the traditional C to Ku frequency bands currently in use are progressively becoming more and more crowded, whereas there is still a need for new services

Manuscript received May 17, 2018; revised December 19, 2018; revised March 19, 2019; accepted April 15, 2019. Date of publication XXX XX, 201X; date of current version XXX XX, 201X. This work was partially supported by the Fonds de la Recherche Scientifique–FNRS under grant FRFC T.1049.15 (NEWPORT), and by the European Space Agency (ESA) under the contract ESA4000113886/15/NL/LVH. The Alphasat Aldo Paraboni experiment at Spino d’Adda is being supported by the Agenzia Spaziale Italiana (ASI).

L. Quibus and D. Vanhoenacker-Janvier are with the Institute of Information and Communication Technologies, Electronics and Applied Mathematics (ICTEAM), Université catholique de Louvain (UCLouvain), 1348 Louvain-la-Neuve, Belgium (e-mail: laurent.quibus@uclouvain.be; danielle.vanhoenacker@uclouvain.be).

L. Luini and C. Riva are with the Dipartimento di Elettronica, Informazione e Bioingegneria (DEIB), Politecnico di Milano (PoLiMi), 20133 Milano, Italy and also with the Istituto di Elettronica e di Ingegneria dell’Informazione e delle Telecomunicazioni (IEITT), Consiglio Nazionale delle Ricerche (CNR), 20133 Milano, Italy (e-mail: lorenzo.luini@polimi.it; carlo.riva@polimi.it).

Color versions of one or more of the figures in this paper are available online at <http://ieeexplore.ieee.org>.

Digital Object Identifier 10.1109/TAP.201x.xxx

or research applications. Secondly, desirable properties such as a higher data rate and a better antenna directivity [1] can be achieved by moving to Ka and Q/V bands. The main drawbacks of high frequencies are the stronger propagation impairments due to the atmosphere. Not only rain, but also turbulence, clouds, and gases, become susceptible to non-negligibly attenuate the signal. The design of systems and coding techniques to overcome those impairments thus requires an accurate characterization of the propagation effects.

EM wave propagation experiments consist in single-frequency beacons aboard satellites and ground stations receiving the emitted signals. Examples of past campaigns include OTS [2], SIRIO [3], OLYMPUS [4], ACTS [5] and ITALSAT [6], [7]. An on-going campaign is the Alphasat TDP5 Aldo Paraboni scientific experiment (SCIEX) [8]. It involves two propagation beacons at the following frequencies:

- 19.701 GHz, linear vertical, boresight at (32.5°N, 20°E);
- 39.402 GHz, linear 45°, boresight at (45.4°N, 9.5°E).

Alphasat is a geosynchronous satellite located at 25°E. Due to its inclined orbit, a tracking system is needed to receive its signal. This paper uses the co-polar beacon signal power level measured at the Spino d’Adda receiving station [9], at both frequencies. Spino d’Adda is located at the 39.402 GHz antenna boresight which means that, on average, the signals is received at 159° in azimuth and 35.5° in elevation. The station is equipped with a multi-channel microwave radiometer, also pointing towards Alphasat.

Processing the beacon signals typically consists in extracting the excess attenuation, i.e. the attenuation due to rain and turbulence. If the total tropospheric attenuation, i.e. also including gases and clouds, is to be derived, then the nonrainy attenuation component must be estimated independently.

Brightness temperature measurements from a microwave radiometer at multiple frequencies permit to accurately estimate the nonrainy attenuation, after the calibration of a retrieval procedure [10]–[12]. However, due to the cost of the equipment, some experimenters, such as some members of the ASALASCA consortium [13], [14], do not operate one. Therefore, there is a need for other methods to estimate nonrainy attenuation.

Other options to retrieve time series of nonrainy attenuation involve GNSS delays [15], [16], or high-resolution Numerical Weather Predictions (NWPs). Regarding the latter approach, studies related to the link budget of satellite downlinks [17]–

[24] or Deep-Space missions [25], [26] have shown the capability of NWP models to produce time series of propagation effects. This contribution, which extends the work in [27], investigates the use of the Weather Research and Forecasting (WRF) model [28], [29] to support EM wave propagation campaigns with nonrainy attenuation estimates.

In the following, Sec. II outlines the procedure to extract the tropospheric attenuation from the measured beacon signals. It highlights why a nonrainy attenuation estimate is necessary. Then, Sec. III introduces the electromagnetic models underpinning the estimation of the nonrainy attenuation. They take as input the pressure, temperature, humidity, and cloud liquid water content. This latter parameter can itself be estimated from the others via cloud detection algorithms, presented in Sec. IV. All those models intervene also in the calibration of the radiometric attenuation recovery, as summarized in Sec. V, and in the processing of WRF data, as described in Sec. VI. The main results of this paper are reported in Sec. VII. They show a comparison between nonrainy attenuation estimated with a radiometer or using WRF, for four months of data collected at the Spino d'Adda Alphasat station.

II. EM WAVE ATTENUATION MEASUREMENTS IN PROPAGATION EXPERIMENTS

This section illustrates the processing of the measured beacon signals in a propagation experiment. It emphasizes that the total attenuation is the desired outcome, while showing why only the contributions of rain and scintillation are extracted.

A. Measured Beacon Signal Power and Total Attenuation

The power P_r (W) received from the satellite beacon at the ground station is usually expressed with respect to a reference power P_0 (W) as the received power level L_r such that

$$L_r = 10 \log_{10} \left(\frac{P_r}{P_0} \right) \quad (1)$$

and, in the case of Spino, $P_0 = 1 \text{ mW}$ so that L_r is expressed in dBm. The value of L_r depends on the whole system and is not a universal metric of the atmospheric attenuation. Indeed, such a metric is the total attenuation A_{tot} (dB) given by

$$A_{tot} = -10 \log_{10} \left(\frac{P_r}{P_{na}} \right) \quad (2)$$

where P_{na} (W) is the received power in hypothetical conditions of absence of the atmosphere. In practice, however, P_{na} cannot be known with high accuracy [10], [12], as it also depends on several system parameters that might vary in time.

B. Identification of Precipitation Events and Extraction of the Excess Attenuation from the Measured Beacon Signal

The upper part of Fig. 1 displays a time series of L_r . There is a drop of about 1 dBm between midnight and noon which is attributable mainly to the satellite motion. The fast variations of the signal are characteristically scintillation. In the evening, the marked negative peak is due to a rain event.

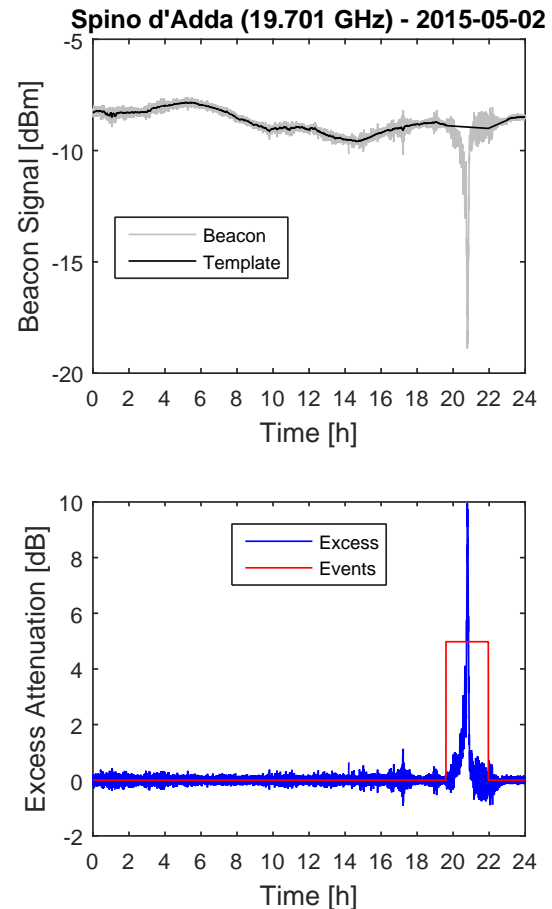


Fig. 1. Example of rain event identification, template construction, and excess attenuation extraction from the Alphasat Ka signal collected at Spino d'Adda.

Thanks to their noticeable features, rain events can be flagged either by visual inspection or by means of some semi-automatic methods. Thanks to its spectral properties, scintillation can be removed by a low-pass filter [30], [31]. Finally, slow-varying tropospheric effects (e.g. the fade induced by gases and clouds) are however hardly identifiable.

The processing of the beacon signal, as depicted in Fig. 1, implies the construction of a template where, during rain events, L_r is replaced by a linear interpolation and the scintillation is filtered out. In other words, this template is the level L_{nr} of the power P_{nr} that would have been measured without rain and turbulence. By subtracting the beacon signal from the template, we obtain the excess attenuation A_{exc} (dB)

$$A_{exc} = L_{nr} - L_r = -10 \log_{10} \left(\frac{P_r}{P_{nr}} \right) \quad (3)$$

a metric including only the effects of rain and turbulence. The relation between A_{exc} and A_{tot} is, from (2) and (3),

$$A_{tot} = A_{exc} + A_{nr} \quad (4)$$

$$A_{nr} = -10 \log_{10} \left(\frac{P_{nr}}{P_{na}} \right) \quad (5)$$

where the nonrainy attenuation A_{nr} (dB) appears as a quantity that must be estimated independently from the beacon signal in order to obtain the total attenuation.

III. NONRAINY ATTENUATION MODELS

This section briefly presents the electromagnetic models used to estimate the attenuations due to gases and clouds.

A. Specific Attenuation

For a uniform plane wave at frequency f (GHz), the attenuation A (dB) along a slant path of length S (km) is

$$A(f) = \int_0^S \gamma(f, s) ds \quad (6)$$

where γ (dB km⁻¹) is the specific attenuation at a distance s (km) from the ground station, along the link. γ is given by

$$\gamma(f, s) = 0.182fN''(f, s) \quad (7)$$

where $N''(f, s)$ (ppm) is the imaginary part of the tropospheric refractivity [32]. Individual contributions to γ can be summed.

B. Specific Attenuation due to Atmospheric Gases

One part of the nonrainy attenuation is due to gases. Recommendation ITU-R P.676-10 [33] provides line-by-line or approximated models to estimate the contributions from dry air (mostly oxygen) $\gamma_O(f)$ and water vapour $\gamma_V(f)$. The required inputs are the pressure, temperature, and humidity.

C. Specific Attenuation due to Clouds

A second part of the nonrainy attenuation is due to clouds. Recommendation ITU-R P.840-7 [34], [35] provides a model, based on Rayleigh scattering by water droplets, to estimate the specific attenuation induced by clouds, $\gamma_L(f)$. The required inputs are the pressure, temperature, and liquid water content.

IV. CLOUD LIQUID WATER CONTENT MODELS

As measurements of the cloud liquid content are not common, algorithms that estimate it from available atmospheric profiles are useful. This section presents two such models.

A. Salonen Cloud Model

The Salonen model [36], modified by [37], receives as input vertical profiles of pressure p , temperature T , and relative humidity RH , and provides as output, profiles of the liquid water content LWC . Cloudy conditions are identified when $RH > RH_c$, with

$$RH_c = 1 - \alpha\sigma(1 - \sigma)(1 + \beta(\sigma - 0.5)), \quad (8)$$

$\alpha = 1$, $\beta = \sqrt{3}$, and $\sigma = p/p_s$ where p_s is the ground pressure. Then, the total water content TWC at the altitude h in the cloud is calculated as

$$TWC = \begin{cases} w_0 \left(\frac{h-h_b}{h_r}\right)^a (1 + cT) & T \geq 0^\circ\text{C} \\ w_0 \left(\frac{h-h_b}{h_r}\right)^a \exp(cT) & T < 0^\circ\text{C} \end{cases} \quad (9)$$

with $w_0 = 0.17 \text{ g m}^{-3}$, $a = 1$, $c = 0.04^\circ\text{C}^{-1}$, $h_r = 1.5 \text{ km}$, and where h_b is the cloud base. Finally,

$$LWC = TWC f_w \quad (10)$$

$$f_w = \begin{cases} 1 & T \geq 0^\circ\text{C} \\ 1 + T/20 & -20 \leq T < 0^\circ\text{C} \\ 0 & T < -20^\circ\text{C} \end{cases} \quad (11)$$

where f_w is the liquid water fraction.

B. Mattioli Cloud Model

The Mattioli model [38] aims to improve the Salonen model. Firstly, although it still makes use of (8) to define the critical relative humidity, its parameters are changed to $\alpha = 0.59$ and $\beta = 1.37$. Secondly, TWC is given by

$$TWC = cz^a(1 - z^{a+1})^b \quad (12)$$

introducing a dependency on the cloud thickness ΔH with

$$c = \begin{cases} 0.8RH & \Delta H < 0.1 \text{ km} \\ 1.46RH\Delta H & 0.1 \text{ km} \leq \Delta H < 0.6 \text{ km} \\ 0.74RH & \Delta H > 0.6 \text{ km} \end{cases}, \quad (13)$$

$z = (h - h_b)/\Delta H$, $a = z/1.5$, and $b = 1.5 + z/1.5$. Thirdly, the expression for the liquid water fraction changes to

$$f_w = \begin{cases} 1 & T \geq 0^\circ\text{C} \\ 1 - (T/35)^2 & -35 \leq T < 0^\circ\text{C} \\ 0 & T < -35^\circ\text{C} \end{cases} \quad (14)$$

whereas LWC is still calculated as in (10).

V. ESTIMATION OF NONRAINY ATTENUATION FROM RADIOMETRIC MEASUREMENTS

This section explains how nonrainy attenuation is estimated from radiometric measurements.

A. Brightness Temperature and Radiometric Attenuation

Assuming that the atmosphere acts as a black-body at the frequency f , a radiometer measures the brightness temperature T_b (K) which can be defined as [32]

$$T_b(f) = T_c\Gamma(f, \infty) + T_{mr}(f)(1 - \Gamma(f, \infty)) \quad (15)$$

where $T_c = 2.7 \text{ K}$ is the cosmic background temperature, T_{mr} (K) is the mean radiative temperature given by

$$T_{mr}(f) = \frac{\int_0^\infty T(s)\gamma(f, s)\Gamma(f, s)ds}{\int_0^\infty \gamma(f, s)\Gamma(f, s)ds}, \quad (16)$$

and where

$$\Gamma(f, s) = \exp\left(-\frac{\ln 10}{10} \int_0^s \gamma(f, s')ds'\right) \quad (17)$$

is the transmission factor. From (6) and (17) it is clear that $\Gamma(f, \infty) = 10^{-0.1A(f)}$ and, as a consequence from (15),

$$A(f) = 10 \log_{10} \left(\frac{T_{mr}(f) - T_c}{T_{mr}(f) - T_b(f)} \right) \quad (18)$$

i.e. measurements of T_b can be used to retrieve the tropospheric attenuation. It is worth highlighting that the equations above are valid under the assumption of scatter-free atmosphere, i.e. when the fade is only due to the absorption by the tropospheric constituents or, in other words, in absence of rain. At this stage, two problems still need to be addressed: firstly, T_{mr} is not a measured quantity, and, secondly, there might not be any radiometric channel centered around the beacon frequency f (as in the case of the Alphasat propagation experiment at Spino d'Adda).

TABLE I
CHARACTERISTICS OF SPINO D'ADDA RADIOMETER FOR ATTENUATION RETRIEVAL ($a_0(19.701 \text{ GHz}) = 0.017, a_0(39.402 \text{ GHz}) = -0.038$)

f_i (GHz)	23.84	27.84	31.4	51.26	52.28
$a_i(19.701 \text{ GHz})$	0.247	0.970	-0.517	0.010	-0.005
$a_i(39.402 \text{ GHz})$	0.040	-0.875	1.989	0.107	-0.033

B. Calibration of the Radiometric Attenuation Retrieval

The procedure to retrieve $A(f_j)$, from measurements of $T_b(f_i)$ at multiple frequencies $f_i \neq f_j$, is detailed in [10]–[12]. The approach uses multiple years of radio-soundings (RAOBS) profiles of p , T and RH collected in a site close to where the radiometer is installed. Firstly, the Salonen model (see Sec. IV-A) is used to estimate the liquid water content LWC . Secondly, for each vertical profile, the following quantities are computed using, e.g., the MPM93 model [32]:

- for f_j and each f_i , the specific attenuations due to oxygen γ_O , water vapour γ_V , and clouds γ_L , then summing their contributions to get γ , similarly to Sec. III,
- for f_j and each f_i , the zenithal nonrainy attenuation A , as given from γ in (6),
- for each f_i , the mean radiative temperature T_{mr} , as given from T and γ in (16),

The conversion from zenithal attenuations to attenuations along a slant path at a given elevation is achieved using the cosecant law, which assumes a stratified atmosphere. T_{mr} varies little over time or elevation and can be approximated by its monthly means $\bar{T}_{mr}(f_i)$ with an acceptable error [12]. It enables the estimation of $A(f_i)$ from $T_b(f_i)$ using (18).

The problem of $f_j \neq f_i$ is then solved by combining linearly multiple radiometric channels [12]

$$A(f_j) \approx a_0(f_j) + \sum_i a_i(f_j)A(f_i) \quad (19)$$

where a_0 and each a_i are obtained by linear regression.

Two channels centered around 20 and 30 GHz are typically sufficient to provide quite an accurate estimate of $A(f_j)$, as they are more sensitive to water vapor and liquid water absorption, respectively. However, more channels are usually employed to increase the accuracy (see Table I for Spino). The regression root-mean-square errors are 0.0006 dB at 19.701 GHz and 0.0029 dB at 39.402 GHz.

C. Accuracy of the Radiometric Attenuation

From [39], the accuracy of the measured radiometric attenuation is the standard deviation of the error ϵ (dB) defined as

$$\epsilon(f) \triangleq A_{nr}^{MWR}(f) - A_{nr}^*(f) \quad (20)$$

where A_{nr}^{MWR} (dB) and A_{nr}^* (dB) are respectively the measured and the true radiometric attenuations given by

$$A_{nr}^{MWR}(f) = 10 \log_{10} \left(\frac{\bar{T}_{mr}(f) - T_c}{\bar{T}_{mr}(f) - T_b(f)} \right) \quad (21)$$

$$A_{nr}^*(f) = 10 \log_{10} \left(\frac{T_{mr}^*(f) - T_c}{T_{mr}^*(f) - T_b^*(f)} \right) \quad (22)$$

TABLE II
AVERAGE MEAN RADIATIVE AND BRIGHTNESS TEMPERATURES USED FOR THE ESTIMATION OF THE RADIOMETRIC ATTENUATION ACCURACY

f_i (GHz)	23.84	27.84	31.4	51.26	52.28
$\bar{T}_{mr}(f_i)$ (K)	274.33	272.11	270.64	269.11	271.23
$\bar{T}_b(f_i)$ (K)	60.75	37.07	35.63	165.96	209.84

with the true temperatures also denoted by an asterisk. It is more convenient to replace the true temperatures T_b^* and T_{mr}^* in (22) by defining the errors in temperature ζ and ξ as

$$\zeta(f) \triangleq T_b(f) - T_b^*(f) \quad (23)$$

$$\xi(f) \triangleq \bar{T}_{mr}(f) - T_{mr}^*(f) \quad (24)$$

whose standard deviations have been estimated. For an ideally calibrated RPG-HATPRO $\sigma_\zeta \approx 0.5 \text{ K}$ [40]; however, due to calibration limitations, in practice, $\sigma_\zeta \approx 2 \text{ K}$ is a more common value [39]. Based on the monthly \bar{T}_{mr} from radio-soundings, $\sigma_\xi \approx 4 \text{ K}$. The error is then a random function $\epsilon(T_b, \zeta, \xi)$ and by linearization around a point $(\bar{T}_b, 0, 0)$ its variance becomes

$$\sigma_\epsilon^2(f) \approx \left(\frac{\partial \epsilon}{\partial \zeta}(f) \right)^2 \sigma_\zeta^2 + \left(\frac{\partial \epsilon}{\partial \xi}(f) \right)^2 \sigma_\xi^2 \quad (25)$$

$$\frac{\partial \epsilon}{\partial \zeta}(f) = \frac{10}{\ln 10} \frac{1}{\bar{T}_{mr}(f) - \bar{T}_b(f)} \quad (26)$$

$$\frac{\partial \epsilon}{\partial \xi}(f) = \frac{10}{\ln 10} \left(\frac{1}{\bar{T}_{mr}(f) - T_c} - \frac{1}{\bar{T}_{mr}(f) - \bar{T}_b(f)} \right) \quad (27)$$

where it has been assumed that the errors $\zeta(f)$ and $\xi(f)$ are independent.

If the attenuation must be retrieved from (19), then

$$\sigma_\epsilon^2(f_j) \approx \sum_i a_i^2 \sigma_\epsilon^2(f_i) + \sum_{k \neq l} a_k a_l \sigma_\epsilon(f_k) \sigma_\epsilon(f_l) r_{kl} \quad (28)$$

where the correlations between the errors at different frequencies r_{kl} are assumed to be nonnegative, i.e. $r_{kl} \in [0, 1]$. From Table I and II, $\sigma_\epsilon \in [0.028, 0.043]$ dB at 19.701 GHz and $[0.050, 0.084]$ dB at 39.402 GHz. The \bar{T}_{mr} in Table II are the yearly average, and the \bar{T}_b are the average of the measurements in nonrainy conditions over four months (see Sec. VII-A).

VI. ESTIMATION OF NONRAINY ATTENUATION FROM NUMERICAL WEATHER PREDICTION MODELS

This section shows how the nonrainy attenuation can be estimated from a Numerical Weather Prediction (NWP) model in the absence of local radiometric measurements.

A. Weather Research and Forecasting: Inputs and Setup

The Weather Research and Forecasting (WRF) model is a public domain Numerical Weather Prediction (NWP) software, and its Advanced WRF (ARW) core is a non-hydrostatic Eulerian solver on an Arakawa C-grid [28], [29]. The goal of running WRF here is to reproduce past atmospheric states to be used as suitable inputs to propagation models. The initialization data comes from the European Centre from Medium-Range Weather Forecasts (ECMWF) operational analysis stage

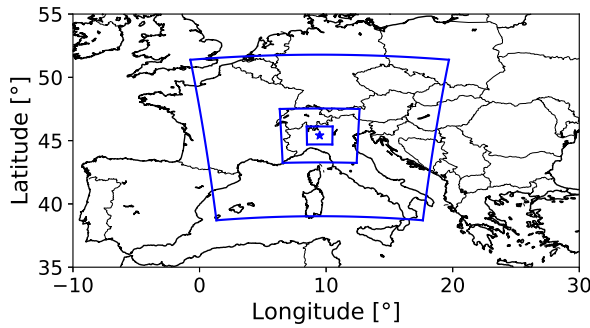


Fig. 2. WRF nested 79×79 Lambert conformal conic domains at 18 km, 6 km and 2 km, respectively, around Spino d'Adda (45.41°N , 9.49°E).

[41], available every 6 h, on pressure and surface levels, and on a 0.125° latitude-longitude grid [42].

For this work, WRF uses daily runs with a 12 h spin-up period. Fig. 2 shows the Lambert conformal conic simulation domains for Spino d'Adda: the resolution increases from 18 km to 2 km after applying two consecutive nests. The innermost domain has a lateral dimension of about 78 km around Spino, offering a sufficient coverage of the troposphere for elevation angles down to 10° . Vertically, there are 50 automatically generated levels going from the ground up to ~ 20 km (50 hPa). The model runs with adaptive time steps, varying from 5 s to 30 s in the 2 km domain, according to the Courant–Friedrichs–Lewy condition, and with $\times 3$ and $\times 9$ scaling factors for the larger domains.

Since this paper aims to reproduce nonrainy conditions, special attention is given to the cloud parametrization and the water microphysics. Two cases are considered:

- Tiedtke and WSM6. The cumulus scheme is disabled at 2 km as clouds are assumed to be resolved. Previous results [27] showed an apparent underestimation of clouds.
- Grell-Freitas and WDM6. The cumulus scheme is scale-aware and kept activated. Double moments are tested as a means to alleviate the cloud underestimation [43].

Other WRF 3.7.1 non-default configuration options are: RRTM longwave and Dudhia shortwave radiations, Yonsei University boundary layer with 2D Smagorinsky diffusion, revised Monin-Obhukov surface layer, thermal diffusion in the soil, and diffusive damping near the top.

B. Attenuation Prediction from NWP Output Data

WRF outputs the pressure, temperature, humidity and cloud liquid water content every 5 min on a 3D grid.

The first post-processing step is to compute γ_O , γ_V , γ_L as explained in Sec. III, on the WRF grid. Alternatively, the cloud liquid water content is found from the Salonen and Mattioli models presented in Sec. IV, yielding other estimates of γ_L .

The second step is to interpolate specific attenuations. Firstly, a vertical interpolation at each horizontal grid point, from the pressure coordinate to fixed altitudes. Secondly, an interpolation to azimuth-elevation-range around the station.

The third step is to integrate the specific attenuations along the range as in (6). Finally, A_{nr} is calculated as the sum of A_O , A_V and A_L .

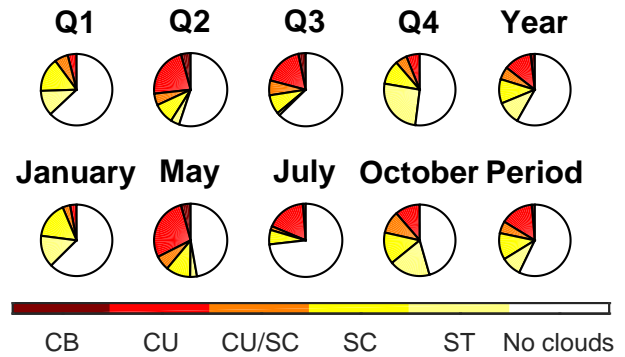


Fig. 3. Proportions of low clouds observed at Milano Linate Airport in 2015 (CB = cumulonimbus, CU = cumulus, SC = stratocumulus, ST = stratus).

VII. COMPARISON OF NONRAINY ATTENUATION ESTIMATES FROM NWP AND RADIOMETRIC DATA

This final section includes the experimental results, assessing how close to a radiometer the nonrainy attenuation estimates from NWP are. The comparison is for four months of Alphasat beacon and radiometric data collected at Spino d'Adda at the sampling rates of 16 Hz and 1 Hz respectively.

A. Selection of the Data for the Comparison

The following months in 2015, given with the data availability and occurrence of rain, are selected for the comparison:

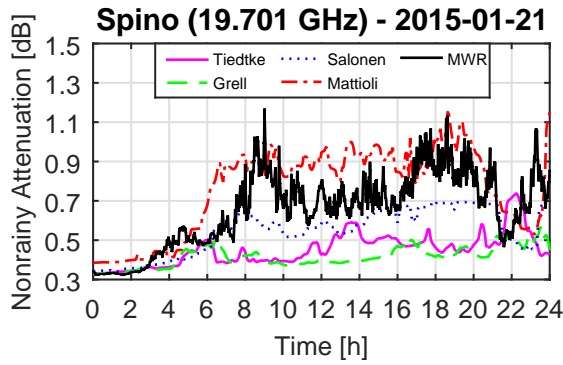
- January (97.4 %, 0.36 % rain), a cloudy and foggy winter month, with some light rain and an event on the 17th.
- May (95.3 %, 1.64 % rain), a rainy spring month with high attenuations from showers and thunderstorms.
- July (89.9 %, 0.10 % rain), a mostly dry and clear-sky summer month, with one thunderstorm on the 25th.
- October (86.9 %, 2.94 % rain), a rainy autumn month.

As a way to evaluate if the chosen months represent the local weather sufficiently well, Fig. 3 illustrates the characteristics of the low clouds cover observed at the Milano Linate Airport (~ 20 km from Spino d'Adda) in 2015 [44]. July has a noticeably clearer sky than its containing quarter, while on the other hand May and October have more convective clouds than their respective quarters. Ultimately, none of the cloud type fractions differs by more than 2.5 % between the year and the four months period, so it can be concluded that this period offers representative cloudy conditions.

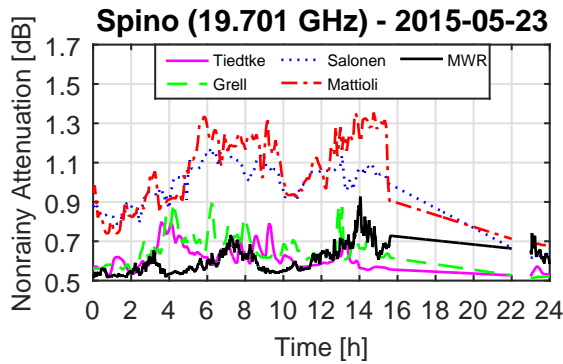
B. Examples of Nonrainy Attenuation Time Series

Fig. 4 shows some examples of 19.701 GHz nonrainy attenuation estimated either with the microwave radiometer (MWR), as explained in Sec. V, or with the NWP model, as explained in Sec. VI.

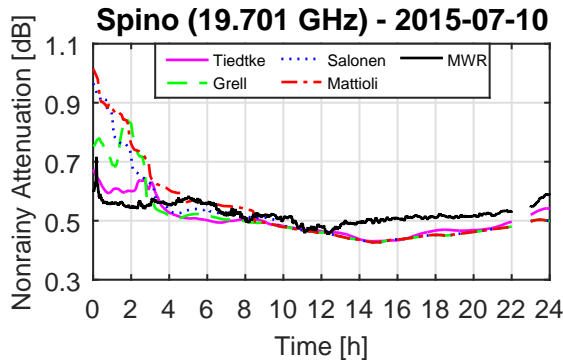
In Fig. 4 (a), for the 21/01/2015, the nonrainy attenuation estimate from the radiometer starts to increase at around 4 am from a base value of ~ 0.35 dB, with peaks around 9 am, 6:30 pm and 11:30 pm, reaching up to 1.2 dB. The NWP curves using the Tiedtke and Grell-Freitas parametrizations present some cloud attenuation peaks but are below the radiometer. The NWP curves using the Salonen and Mattioli models get



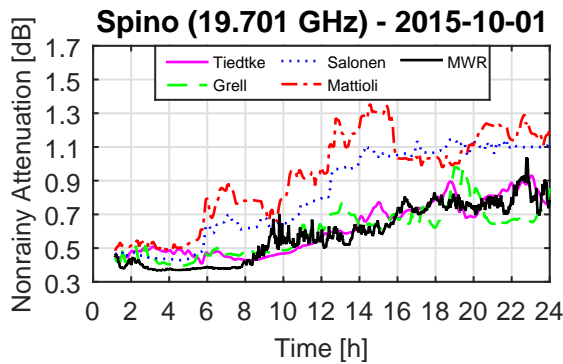
(a) 21st January 2015



(b) 23rd May 2015



(c) 10th July 2015



(d) 1st October 2015

Fig. 4. Examples of Spino d'Adda Alphasat 19.701 GHz nonrainy attenuation time series. Nonrainy attenuation is estimated from a radiometer (MWR) or from WRF. There are four separate WRF results: Tiedtke + WSM6 or Grell-Freitas + WDM6, and the latter with either the Salonen or Mattioli model.

closer, with some overestimation by the Mattioli model. Based on the Linate reports and the rain gauge at Spino, this day has a mix of overcast stratiform clouds and some light rain (up to 2.5 mm h^{-1}) starting around 8 am. This is a situation where defining flags is difficult, because the events last so long. For the radiometer, (18) can be assumed to still hold despite the presence of some scatterers [12]. But for the NWP estimates, the light rain is not modelled; this explains the deviations.

In Fig. 4 (b), for the 23/05/2015, a rain event occurs at the end of the day and, as shown by the linear interpolation, is taken out. Tiedtke and Grell-Freitas follow the radiometer trend well, though not with a very good match on an instantaneous basis. Here, Salonen and Mattioli largely overestimate the nonrainy attenuation. Linate reports suggest the sky has a medium cover of altocumuli throughout the day, and that cumuli start to form around noon and persist during the event.

In Fig. 4 (c), for the 10/07/2015, the sky appears mostly clear, but at the very beginning of the day. The Tiedtke model has the most reasonable behaviour, whereas the other models overestimate the radiometer in the first 3 hours by up to 0.3 dB. The observations point to the presence of only a few scattered (strato-)cumuli and no clouds in the afternoon.

In Fig. 4 (d), for the 01/10/2015, the radiometer estimate is at $\sim 0.35 \text{ dB}$ in the early morning and starts to rise after 8 pm. The Tiedtke and Grell-Freitas models behave similarly. The Salonen and Mattioli models once more overestimate the cloud attenuations. Here the cloud reports describe the progressive build-up of an overcast of stratocumuli and altocumuli.

From these examples, the NWP nonrainy attenuation estimated directly from the NWP models shows cloud peaks similar in amplitude to the radiometer, albeit with some temporal shifts. The Salonen and Mattioli cloud detection algorithms appear to most often overestimate the cloud attenuation, especially near rainy periods. In order to see the broader picture, the next section investigate the long term errors figures.

C. Errors on Nonrainy Attenuation Time Series

The instantaneous error ϵ^{NWP} (dB) of an NWP nonrainy attenuation estimate A_{nr}^{NWP} (dB) with respect to the nonrainy radiometric attenuation A_{nr}^{MWR} (dB) is given by

$$\epsilon^{NWP} \triangleq A_{nr}^{NWP} - A_{nr}^{MWR} = A_{tot}^{NWP} - A_{tot}^{MWR} \quad (29)$$

where by (3) ϵ^{NWP} is also the error on the total attenuations A_{tot}^{NWP} and A_{tot}^{MWR} , as in both cases the excess attenuation is the same. A relative error ϵ_r^{NWP} (%) is also defined as

$$\epsilon_r^{NWP} \triangleq 100 (\epsilon^{NWP} / A_{nr}^{MWR}) \quad (30)$$

where $A_{nr}^{MWR} > 0$ as it does not include scintillation.

The following error figures are then investigated

- the mean error (ME) on ϵ^{NWP} or ϵ_r^{NWP} ,
- the root mean square error (RMSE) on ϵ^{NWP} or ϵ_r^{NWP} ,
- the correlation ρ^{NWP} between A_{nr}^{NWP} and A_{nr}^{MWR} .

Table III lists the error figures for the four months under study, at both 19.701 GHz (Ka band) and 39.402 GHz (Q band), with the best individual figures in bold.

TABLE III

ERRORS (ABSOLUTE AND RELATIVE) AND CORRELATION OF ALPHASAT NONRAINY ATTENUATION ESTIMATED FROM AN NWP MODEL WITH RESPECT TO THE MICROWAVE RADIOMETER (MWR), FOR DIFFERENT TYPES OF NWP ATTENUATION ESTIMATES (BEST IN BOLD)

Period	NWP vs MWR	19.701 GHz (Ka-band)				39.402 GHz (Q-band)			
		Type of NWP nonrainy attenuation estimate							
		Tiedtke	Grell-Freitas	Salonen	Mattioli	Tiedtke	Grell-Freitas	Salonen	Mattioli
January	RMSE (dB) [%]	0.09 [15.5]	0.09 [15.8]	0.08 [17.1]	0.11 [24.7]	0.26 [19.3]	0.26 [21.4]	0.26 [23.6]	0.37 [40.9]
	ME (dB) [%]	-0.03 [-5.5]	-0.02 [-4.3]	-0.01 [-2.9]	0.02 [3.9]	-0.09 [-7.9]	-0.05 [-4.7]	-0.03 [-2.5]	0.09 [9.4]
	ρ^{NWP} (-)	0.808	0.805	0.823	0.842	0.607	0.596	0.658	0.725
May	RMSE (dB) [%]	0.11 [17.4]	0.12 [18.6]	0.19 [29.3]	0.23 [37.3]	0.28 [26.1]	0.31 [29.5]	0.57 [59.4]	0.76 [80.6]
	ME (dB) [%]	-0.04 [-6.5]	-0.03 [-4.8]	0.06 [8.6]	0.09 [13.6]	-0.09 [-7.5]	-0.05 [-5.1]	0.26 [26.4]	0.38 [39.0]
	ρ^{NWP} (-)	0.725	0.678	0.714	0.677	0.315	0.282	0.573	0.542
July	RMSE (dB) [%]	0.13 [16.0]	0.14 [17.3]	0.14 [17.9]	0.14 [17.9]	0.17 [16.1]	0.20 [19.2]	0.26 [24.5]	0.26 [25.3]
	ME (dB) [%]	-0.05 [-6.5]	-0.05 [-6.0]	-0.03 [-3.9]	-0.03 [-4.0]	-0.05 [-5.2]	-0.04 [-3.8]	0.02 [2.5]	0.02 [2.2]
	ρ^{NWP} (-)	0.608	0.571	0.573	0.562	0.380	0.320	0.383	0.359
October	RMSE (dB) [%]	0.11 [17.3]	0.13 [21.3]	0.15 [24.3]	0.17 [30.2]	0.32 [25.6]	0.41 [36.2]	0.41 [38.9]	0.52 [53.6]
	ME (dB) [%]	-0.01 [-0.9]	-0.01 [0.4]	0.05 [9.6]	0.07 [12.3]	-0.08 [-5.2]	-0.05 [-2.2]	0.17 [17.1]	0.23 [23.3]
	ρ^{NWP} (-)	0.788	0.705	0.818	0.779	0.631	0.478	0.767	0.716
4 months	RMSE (dB) [%]	0.11 [16.5]	0.12 [18.3]	0.15 [22.7]	0.17 [28.5]	0.26 [22.2]	0.31 [27.2]	0.40 [39.6]	0.51 [54.4]
	ME (dB) [%]	-0.03 [-4.9]	-0.03 [-3.8]	0.02 [2.8]	0.04 [6.4]	-0.08 [-6.5]	-0.05 [-2.2]	0.10 [10.8]	0.18 [18.6]
	ρ^{NWP} (-)	0.878	0.849	0.826	0.791	0.590	0.502	0.637	0.618

For January, the NWP estimates with Tiedtke, Grell-Freitas and Salonen show very similar performances, and all have negative ME. The RMSE is below 0.1 dB in Ka band and below 0.3 dB in Q band. ρ^{NWP} is around 0.8 in Ka band and down to 0.6 in Q band. The Salonen model is the overall best with the lowest ME, but not by a very significant margin. The Mattioli RMSE is the worst, by 0.1 dB at Q band, and it has a slightly positive ME, but it has the highest ρ^{NWP} .

For May, the Tiedtke model is the best in RMSE: 0.11 dB in Ka band and 0.28 dB in Q band. The Grell-Freitas model is similar while slightly better in ME. The NWP estimates using the Salonen and Mattioli models perform far less favourably: as pointed out by their large positive ME, they largely overestimate the clouds. This is understandable given that their critical humidity threshold are designed for nonrainy periods, yet May 2015 was a very rainy month. The correlations are here around 0.7 in Ka band and around 0.3 or 0.55 in Q band for the Tiedtke/Grell-Freitas or Salonen/Mattioli results respectively.

For July, the Tiedtke model is once again the best in RMSE with 0.13 dB in Ka band, and no more than 0.17 dB in Q band. The performances of the other models are not too far from that however. The Salonen and Mattioli models actually provide the best ME, and in Q band they have a slightly positive ME. The correlations are however especially poor, around 0.6 and 0.35.

For October, the Tiedtke model is also the overall best, with the Grell-Freitas model being worst in RMSE and ρ^{NWP} . As for May, the Salonen and Mattioli model have high RMSE and ME, though they maintain a better correlation in Q band.

Looking at the four months together, the best model appears to be Tiedtke with RMSEs of 0.11 dB (Ka) and 0.26 dB (Q). This is 3 to 5 times higher than the radiometric accuracy estimated in Sec. V-C. As another reference point, [16] proposes a 0.165 dB threshold for the agreement between MWR and GNSS as a way to detect malfunctions of the radiometer at 19.7 GHz and for clear-sky conditions. In that regard, the

RMSEs found here are large (and also as relative values $\sim 15 - 25$ %) yet physically acceptable. The Grell-Freitas model performs similarly to Tiedtke, but the Salonen and Mattioli models are confirmed to overestimate the cloud attenuation, particularly close to rainy periods, and especially the Mattioli model. Part of the overestimation may be explained by the not so high number (i.e. 50) of vertical levels used for WRF, yielding larger apparent cloud thicknesses.

To understand the correlations, water vapour is typically correlated > 0.9 between MWR/GNSS/RAOBS/NWP data, though there is some seasonal variability and values ~ 0.7 were observed with NWP models in summer [15]. For the NWP nonrainy attenuation estimates, the presence of the clouds reduces the correlation with the radiometer, as the cloud events are not always predicted at the right time (see e.g. Fig. 4 (b)). Because the cloud attenuation increases faster with the frequency, its contribution degrades the correlation further at Q band. The especially poor correlations in May and July suggest indeed difficulties during the warmer seasons and/or regarding convective clouds, present in majority during those months. Cases when light rain is mixed with clouds and not flagged (see e.g. Fig. 4 (d)) also negatively affect the correlation.

For the purpose of obtaining the total attenuation from the NWP estimates, an important point to consider here is also the accuracy of the excess attenuation. With a procedure similar to II-B, the retrieval accuracy is estimated to be $\sim 0.2 - 0.5$ dB in the 20 – 50 GHz band [7]. In that regard, it appears that the results, at least those from the Tiedtke/Grell-Freitas models, are realistic enough to be considered statistically.

D. Error on Total Attenuation Statistics

Ultimately, what is expected as the primary output of a propagation experiment is the Complementary Cumulative Distribution Function (CCDF) of the total attenuation. Some

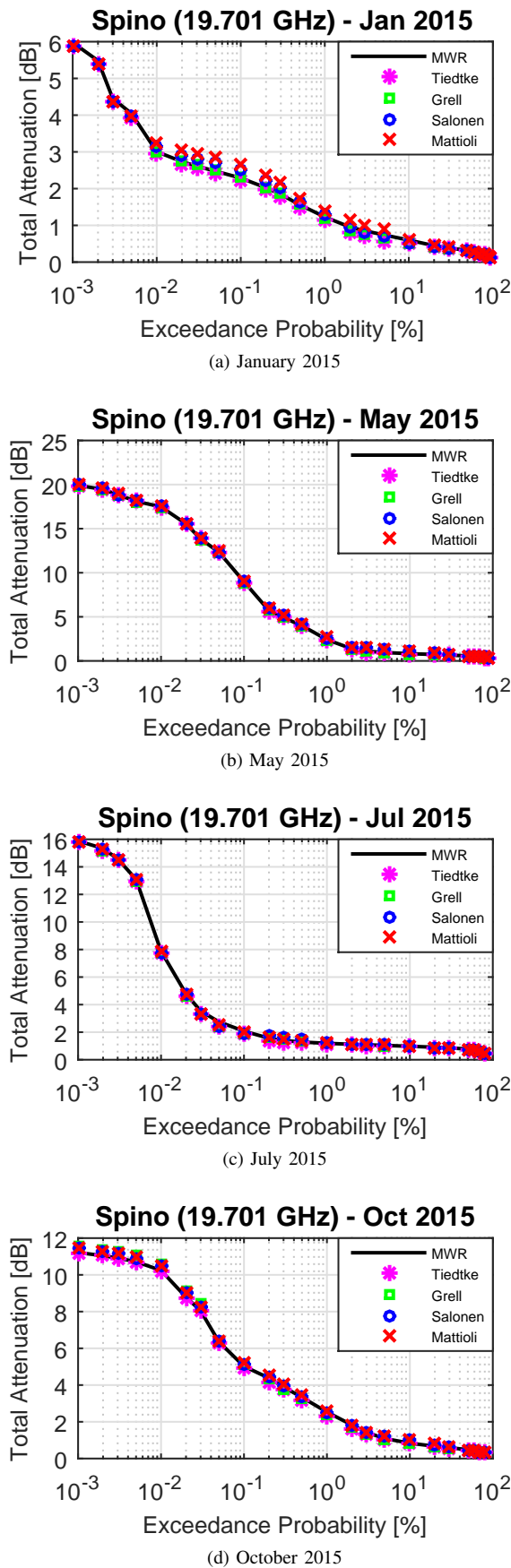


Fig. 5. Spino d'Adda Alphasat 19.701 GHz total attenuation monthly CCDFs. Nonrainy attenuation is estimated from a radiometer (MWR) or from WRF. There are four separate WRF results: Tiedtke + WSM6 or Grell-Freitas + WDM6, and the latter with either the Salonen or Mattioli model.

standardized details of the CCDF computation are within the ITU-R SG3 Table II-1 template [45]. Notably, the CCDFs must be normalized with respect to the total observation period, here one month, and not the total number of available samples.

Fig. 5 shows the comparison of the 19.701 GHz CCDFs, for the four months, for the radiometer and the NWP models. The description includes the values for Ka/Q band.

In Fig. 5 (a), for January, the mostly cloudy conditions and the absence of strong rain events highlight differences between the different NWP models. The Tiedtke model follows the radiometric curve with a small underestimation over the whole probability range reaching -20% / -30% (-0.2 dB/ -0.6 dB) between 1 and 10 %. Grell-Freitas is slightly above Tiedtke. The Salonen and Mattioli models present an overestimation of the central part of the radiometric curve, Mattioli being above Salonen, with respective errors around 10 %/15 % (0.2 dB/ 0.8 dB) and 20 %/25 % (0.4 dB/ 1.4 dB) for 10^{-1} %.

In Fig. 5 (b), for May, the Tiedtke model has an error of -10% / -20% (-0.1 dB/ -0.4 dB) between 1 and 10 %, while Grell-Freitas is slightly above it until 10^{-1} %. The Salonen and Mattioli models on the contrary overestimate that part of the curve, with errors up to 40 %/90 % (0.4 dB/ 1.1 dB) and 45 %/120 % (0.4 dB/ 1.5 dB) near 10 % of the time.

In Fig. 5 (c), for July, the curves remains at low attenuation values until the single rain event appears between 10^{-2} and 10^{-1} % where all the NWP results underestimate the radiometer by -10% / -15% (-0.3 dB/ -1 dB). Again for the central part curve, between exceedance probabilities of 10^{-1} and 1 %, the Salonen and Mattioli models overestimate the radiometer by up to about 10 %/45 % (0.15 dB/ 0.9 dB) and 15 %/60 % (0.2 dB/ 1.1 dB) respectively. The Grell-Freitas model has an error of 5 %/30 % (0.05 dB/ 0.5 dB) in the same range, but Tiedtke stays below the radiometer at all probabilities.

In Fig. 5 (d), for October, Tiedtke remains below the radiometer, with its highest relative error -10% (-0.2 dB/ -0.5 dB) between 1 and 10 %. Grell-Freitas is slightly above Tiedtke and has an error up to 5 % (0.4 dB/ 1.1 dB) between 10^{-3} and 10^{-1} %, due to misplaced high attenuation NWP cloud events. Both the Salonen and Mattioli models make a similar error of 25 %/45 % (0.2 dB/ 0.7 dB) for 10 % of the time.

From all these observations, the NWP estimates from the Tiedtke and Grell-Freitas cumulus schemes allow to reproduce the monthly CCDFs with a relative error better than $\pm 30\%$ at any reference exceedance probability level. The highest errors are usually located in the 1 to 10 % exceedance probability range, July being the exception. Tiedtke almost never overestimates the radiometer, whereas Grell-Freitas does in a few instances and is almost always above Tiedtke. In the practical view of designing systems or fade mitigation techniques, both schemes are similarly useful, Tiedtke is more consistent but Grell-Freitas introduces a lower risk of underestimation. On the other hand, the NWP estimates from the Salonen and Mattioli cloud detection algorithms can largely overestimate the radiometer anywhere in the 10^{-2} to 10 % probability range. For the Mattioli model, it goes up to 120 % (1.5 dB) for 10 % of the time in May at Q band. Extracted system margins would be safe, but not economically optimal.

VIII. CONCLUSION

In order to obtain the total atmospheric attenuation, propagation experiments require independent estimates of the attenuation in nonrainy conditions. Radiometric measurements are the classic way to tackle the problem. Numerical Weather Prediction data, as input to propagation models, can provide such estimates as well. To this aim, either an appropriate NWP parametrization for the clouds is selected, or a cloud detection algorithm is applied.

The comparisons of NWP-derived against radiometric estimates, using four months of beacon and radiometric data collected at Spino d'Adda, at 16 and 1 samples per second respectively, show the best overall results are obtained with the Tiedtke NWP scheme: the root mean-square errors are 0.11 dB (16.5 %) and 0.26 dB (22.2 %), the mean errors -0.03 dB (-4.9 %) and -0.08 dB (-6.5 %), and the correlations 0.878 and 0.590, at the frequencies of 19.701 GHz and 39.402 GHz respectively. The root mean-square errors are estimated here to be roughly 3 to 5 times higher than the standard deviation of the radiometric attenuation. Other practical estimates of the radiometric accuracy amount typically to ~ 0.1 dB [16]. The correlations are not excellent, but in Ka band they are still commensurable to the correlations > 0.9 observed for water vapour [15]. Analyses of individual NWP nonrainy attenuation time series reveal the cloud events have a poor instantaneous correlation. It explains why the nonrainy attenuation correlation is poorer than what is expected in clear-sky, and why it degrades with increased frequency as the cloud attenuation becomes relatively higher. Despite this, the errors remain acceptable at the statistical level, for the purpose of building the total attenuation distribution, and considering that extracing the excess attenuation in a propagation experiment has an estimated accuracy of $0.2 - 0.5$ dB in the 20-50 GHz band [7]. Indeed, for both the Tiedtke and Grell-Freitas schemes, the relative error on the total attenuation distribution never exceeds ± 30 % for the reference ITU-R exceedance probabilities. On the other hand, the estimates obtained using cloud detection algorithms (proposed by Salonen and Mattioli) strongly overestimate the cloud attenuation, especially near rainy conditions.

In conclusion, using two different NWP parametrizations did not result in very significant differences, while cloud detection algorithms seem too pessimistic when used with the NWP data. Overall, the accuracy of the method can be considered satisfactory for use by the EM wave propagation community, and subsequently to guide satellite system designers. A more careful design of the NWP domains might lower the error further, though part of the appeal of the domains presented in this work is that they are small and automatically defined.

The methodology applied in this paper would still benefit from more tests, by considering both larger time periods and multiple sites. An extension of the study for Spino d'Adda to a full year is being considered. Joanneum Research's Alphasat measurements in Graz are also being considered: preliminary comparisons over the second half of 2017 give error figures similar to the ones in this paper, which shows robustness with respect to different propagation events definition procedures.

This is important since in practice an accurate identification of events without a radiometer is also more difficult.

Applications of the NWP nonrainy attenuation estimates for stations without a radiometer are on-going with the ASALASCA consortium. Perspectives exist also for future propagation experiments or other studies involving non-GEO links, radio-links at even higher frequencies, and optical links.

ACKNOWLEDGMENT

The authors would like to thank Dr Antonio Martellucci from ESA as well as the experimenters of the ASALASCA consortium for fruitful discussions. The authors would also like to thank Dr Nicolas Jeannin from ONERA for sharing the code of their Atmospheric Channel Simulator. The authors would like to acknowledge NCAR for making WRF available and ECMWF as the creator of the initialization data.

REFERENCES

- [1] D. M. Pozar, *Microwave Engineering*, 4th ed. Wiley, 2012.
- [2] P. Sobieski, A. Laloux, and G. Brussaard, "Results of the European Space Agency OTS Propagation Campaign," in *Proc. 14th Eur. Microwave Conf.*, Liège, Belgium, 1984.
- [3] F. Carassa, "The SIRIO programme and its propagation and communication experiment," *Alta Frequ.*, vol. XLVII, no. 4, pp. 65E-71E, 1978.
- [4] B. R. Arbesser-Rastburg and G. Brussaard, "Propagation research in Europe using the OLYMPUS satellite," *Proc. IEEE*, vol. 81, no. 6, pp. 865-875, Jun. 1993.
- [5] R. Bauer, "Ka-Band Propagation Measurements: An Opportunity with the Advanced Communications Technology Satellite (ACTS)," *Proc. IEEE*, vol. 85, no. 6, pp. 853-862, Jun. 1997.
- [6] C. Riva, "Seasonal and diurnal variations of total attenuation measured with the ITALSAT satellite at Spino d'Adda at 18.7, 39.6 and 49.5 GHz," *Int. J. Sat. Comm. Networking*, vol. 22, no. 4, p. 449-476, Jul. 2004.
- [7] S. Ventouras, S. A. Callaghan, and C. L. Wrench, "Long-term statistics of tropospheric attenuation from the Ka/U band ITALSAT satellite experiment in the United Kingdom," *Radio Sci.*, vol. 41, no. 2, Apr. 2006.
- [8] T. Rossi *et al.*, "Satellite Communication and Propagation Experiments Through the Alphasat Q/V Band Aldo Paraboni Technology Demonstration Payload," *IEEE Aerosp. Electron. Syst. Mag.*, vol. 31, no. 3, pp. 18-27, Mar. 2016.
- [9] C. Riva *et al.*, "Preliminary Results from the ASI and NASA Alphasat Experimental Equipment," in *Proc. 22nd Ka and Broadband Communications, Navigation and Earth Observation Conf.*, Cleveland, OH, 2016.
- [10] L. Luini, C. Riva, C. Capsoni, and A. Martellucci, "Attenuation in Nonrainy Conditions at Millimeter Wavelengths: Assessment of a Procedure," *IEEE Trans. Geosci. Remote Sens.*, vol. 45, no. 7, pp. 2150-2157, Jul. 2007.
- [11] L. Luini and C. Capsoni, "Using NWP Reanalysis Data for Radiometric Calibration in Electromagnetic Wave Propagation Experiments," *IEEE Trans. Antennas Propag.*, vol. 64, no. 2, pp. 700-707, Feb. 2016.
- [12] L. Luini, C. Riva, R. Nebuloni, M. Mauri, J. Nessel, and A. Fanti, "Calibration and Use of Microwave Radiometers in Multiple-site EM Wave Propagation Experiments," in *Proc. 12th Eur. Conf. Antennas Propag. (EuCAP)*, London, UK, 2018.
- [13] S. Ventouras *et al.*, "Large Scale Assessment of Ka/Q band Atmospheric Channel Across Europe with ALPHASAT TDP5: A New Propagation Campaign," in *Proc. 10th Eur. Conf. Antennas Propag. (EuCAP)*, Davos, Switzerland, 2016.
- [14] —, "Large Scale Assessment of Ka/Q Band Atmospheric Channel Across Europe with ALPHASAT TDP5: The Augmented Network," in *Proc. 11th Eur. Conf. Antennas Propag. (EuCAP)*, Paris, France, 2017, pp. 1471-1475.
- [15] A. Memmo *et al.*, "Comparison of MM5 integrated water vapor with microwave radiometers, GPS, and radiosonde measurements," *IEEE Trans. Geosci. Remote Sens.*, vol. 43, no. 5, pp. 1050-1058, May 2005.
- [16] G. A. Siles, J. M. Riera, and P. García-del-Pino, "An Application of IGS Zenith Tropospheric Delay Data to Propagation Studies: Validation of Radiometric Atmospheric Attenuation," *IEEE Trans. Antennas Propag.*, vol. 64, no. 1, pp. 262-269, Jan. 2016.

- [17] D. D. Hodges, R. J. Watson, and G. Wyman, "An Attenuation Time Series Model for Propagation Forecasting," *IEEE Trans. Antennas Propag.*, vol. 54, no. 6, pp. 1726–1733, Jun. 2006.
- [18] —, "Initial Comparisons of Forecast Attenuation and Beacon Measurements at 20 and 40 GHz," in *Proc. 1st Eur. Conf. Antennas Propag. (EuCAP)*, Nice, France, 2006.
- [19] M. Outeiral García, N. Jeannin, L. Féral, and L. Castanet, "Use of WRF Model to Characterize Propagation Effects in the Troposphere," in *Proc. 7th Eur. Conf. Antennas Propag. (EuCAP)*, Göteborg, Sweden, 2013, pp. 1377–1381.
- [20] N. Jeannin *et al.*, "Atmospheric Channel Simulator for the Simulation of Propagation Impairments for Ka Band Data Downlink," in *Proc. 8th Eur. Conf. Antennas Propag. (EuCAP)*, The Hague, The Netherlands, 2014, pp. 4170–4174.
- [21] G. Fayon, L. Féral, L. Castanet, N. Jeannin, and X. Boulanger, "Use of WRF to Generate Site Diversity Statistics in South of France," in *32nd URSI GASS*, Montréal, CA, 2017.
- [22] F. Cuervo *et al.*, "Short Term Satellite Channel Characteristics Forecast Using Numerical Weather Prediction Data," in *Proc. 12th Eur. Conf. Antennas Propag. (EuCAP)*, London, U.K., 2018.
- [23] K. Grythe, L. E. Bråten, S. S. Rønning, and T. Tjelta, "Predicting near-time satellite signal attenuation at Ka-band using tropospheric weather forecast model," in *Proc. 12th Eur. Conf. Antennas Propag. (EuCAP)*, London, U.K., 2018.
- [24] C. Kourogorgas, A. Z. Papafragkakis, A. D. Panagopoulos, and S. Ventouras, "Long-Term and Short-Term Atmospheric Impairments Forecasting for High Throughput Satellite Communication Systems," in *Proc. 12th Eur. Conf. Antennas Propag. (EuCAP)*, London, U.K., 2018.
- [25] F. Davarian, S. Shambayati, and S. Slobin, "Deep space Ka-band link management and Mars Reconnaissance Orbiter: long-term weather statistics versus forecasting," *Proc. IEEE*, vol. 92, no. 12, pp. 1879–1894, Dec. 2004.
- [26] M. Biscarini *et al.*, "Optimizing Data Volume Return for Ka-Band Deep Space Links Exploiting Short-Term Radiometeorological Model Forecast," *IEEE Trans. Antennas Propag.*, vol. 64, no. 1, pp. 235–250, Jan. 2016.
- [27] L. Quibus, L. Luini, C. Riva, and Danielle-Vanhoenacker-Janvier, "Numerical Weather Prediction Models for the Estimate of Clear-Sky Attenuation Level in Alphasat Beacon Measurement," in *Proc. 12th Eur. Conf. Antennas Propag. (EuCAP)*, London, U.K., 2018.
- [28] W. Wang *et al.*, "ARW Version 3 Modeling System User's Guide," NCAR, Boulder, CO, Tech. Rep., Jan. 2016.
- [29] W. C. Skamarock *et al.*, "A Description of the Advanced Research WRF Version 3," NCAR, Boulder, CO, Tech. Rep. NCAR/TN-475+STR, Jun. 2008.
- [30] Y. Karasawa and T. Matsudo, "Characteristics of Fading on Low-Elevation Angle Earth-Space Paths with Concurrent Rain Attenuation and Scintillation," *IEEE Trans. Antennas Propag.*, vol. 39, no. 5, pp. 657–661, May 1991.
- [31] E. Maticciani, M. Mauri, and C. Riva, "Relationship between scintillation and rain attenuation at 19.77 GHz," *Radio Sci.*, vol. 31, no. 2, pp. 273–279, 1996.
- [32] H. J. Liebe, G. A. Hufford, and M. G. Cotton, "Propagation modelling of moist air and suspended water/ice particles at frequencies below 1000 GHz," in *Proc. AGARD 52nd Spec. Meeting EM Wave Propag. Panel*, Palma de Maiorca, Spain, 1993.
- [33] International Telecommunication Union-Radiocommunication (ITU-R), "Recommendation ITU-R P.676-10: Attenuation by atmospheric gases," Sep. 2013.
- [34] —, "Recommendation ITU-R P.840-7: Attenuation due to clouds and fog," Dec. 2017.
- [35] H. J. Liebe, T. Manabe, and G. A. Hufford, "Millimeter-Wave and Attenuation and Delay Rates due to Fog/Cloud Conditions," *IEEE Trans. Antennas Propag.*, vol. 37, no. 12, pp. 1617–1623, Dec. 1989.
- [36] E. Salonen and S. Uppala, "New prediction method of cloud attenuation," *Electronic Letters*, vol. 27, no. 12, pp. 1106–1008, Apr. 1991.
- [37] A. Martellucci, J. P. V. Poiars Baptista, and G. Blarzino, "New climatological databases for ice depolarization on satellite radio links," in *Proc. 1st Int. Workshop COST 280 "Propagation Impairment Mitigation for Millimetre Wave Radio Systems"*, Malvern, U.K., 2002.
- [38] V. Mattioli, P. Basili, S. Bonafoni, P. Ciotti, and E. R. Westwater, "Analysis and improvements of cloud models for propagation studies," *Radio Sci.*, vol. 44, no. 2, Mar. 2009.
- [39] F. Barbaliscia *et al.*, "Reference book on radiometry and meteorological measurements," in *OPEX Second Workshop of the OLYMPUS Propagation Experimenters*, Noordwijk, NL, 1994.
- [40] Radiometer Physics GmbH. (2018, Dec.) Humidity And Temperature PROFilers. [Online]. Available: <https://www.radiometer-physics.de/products/microwave-remote-sensing-instruments/radiometers/humidity-and-temperature-profilers/#tabs-container-1>
- [41] European Centre for Medium-Range Weather Forecasts (ECMWF). (2018, Mar.) Set I - Atmospheric Model high resolution 10-day forecast (HRES). [Online]. Available: <https://www.ecmwf.int/en/forecasts/datasets/set-i>
- [42] —. (2018, Mar.) Changes in ECMWF model. [Online]. Available: <https://www.ecmwf.int/en/forecasts/documentation-and-support/changes-ecmwf-model>
- [43] K.-H. Min, S. Choo, D. Lee, and G. Lee, "Evaluation of WRF Cloud Microphysics Schemes Using Radar Observations," *Weather and Forecasting*, vol. 30, no. 6, pp. 1571–1589, Dec. 2015.
- [44] Meteomanz. (2018, Dec.) SYNOP/BUFR observations. Data by hours. [Online]. Available: <http://www.meteomanz.com/sy1?ty=hp&l=1&cou=6260&ind=16080&d1=01&m1=01&y1=2015&h1=00Z&d2=31&m2=01&y2=2015&h2=23Z>
- [45] International Telecommunication Union-Radiocommunication (ITU-R). (2018, Mar.) SG 3 Databanks - Formatted Tables. [Online]. Available: <https://www.itu.int/en/ITU-R/study-groups/rsg3/Pages/dtbank-form-tables.aspx>



Laurent Quibus was born in Belgium in 1992. He received the Master in Physical Engineering from the Université catholique de Louvain in 2015. Since then he has been pursuing a PhD in Engineering and Technology at that same university. His research focuses mostly on the application of Numerical Weather Prediction (NWP) models to estimate the tropospheric impairments on Earth-space radio-links. In particular, he is working with the Weather Research and Forecasting (WRF) software and data from the European Centre for Medium-Range Weather Forecasts (ECMWF). Consequently, he is also interested in comparisons with measurements from propagation beacons, weather radars, radiometers, GNSS stations, ..., and also other NWP models or ITU-R recommendations. Part of those activities are possible thanks to a project in collaboration with the Royal Meteorological Institute of Belgium under a grant from the Fonds de la Recherche Scientifique (FRS-FNRS). He is also involved in ESA contracts, principally with the ASALASCA consortium of Alphasat experimenters.



Lorenzo Luini was born in Italy, in 1979. He received the Laurea Degree (cum laude) in Telecommunication Engineering in 2004 and the Ph.D. degree in Information Technology in 2009 (cum laude) both from Politecnico di Milano, Italy. He is currently a tenure-track Assistant Professor at DEIB (Dipartimento di Elettronica, Informazione e Bioingegneria) of Politecnico di Milano. His research activities are focused on electromagnetic wave propagation through the atmosphere, both at radio and optical frequencies. Lorenzo Luini also worked as a System Engineer in the Industrial Unit – Global Navigation Satellite System (GNSS) Department – at Thales Alenia Space Italia S.p.A. He has been involved in several European COST projects, in the European Satellite Network of Excellence (SatNEx), as well as in several projects commissioned to the research group by the European Space Agency (ESA), the USA Air Force Laboratory (AFRL) and the European Commission (H2020). Lorenzo Luini authored more than 150 contribution to international conferences and scientific journals. He is Associate Editor of International Journal on Antennas and Propagation (IJAP), IEEE Senior Member and member of the Italian Society of Electromagnetism, Board Member of the working group "Propagation" of EurAAP (European Association on Antennas and Propagation) and Leader of Working Group "Propagation data calibration" within the AlphaSat Aldo Paraboni propagation Experimenters (ASAPE) group.



Carlo Riva was born in 1965. He received the Laurea Degree in Electronic Engineering and the PhD degree in Electronic and Communication Engineering, from Politecnico di Milano, Milano, Italy, in 1990 and 1995, respectively. In 1999, he joined the Dipartimento di Elettronica, Informazione e Bioingegneria, Politecnico di Milano, where, since 2006, he has been an Associate Professor of electromagnetic fields. He participated in the Olympus, Italsat and (the running) Alphasat Aldo Paraboni

(for whose propagation experiment he has been appointed Principal Investigator by ASI in 2012) propagation measurement campaigns, in the COST255, COST280 and COSTIC0802 international projects on propagation and telecommunications and in the Satellite Communications Network of Excellence (SatNEx). He supports the ITU-R Study Groups activities and he is Chairman of WP 3J of SG3 ('Propagation fundamentals'). He is the author of about 200 papers published in international journals or international conference proceedings. His main research activities are in the fields of atmospheric propagation of millimeter-waves, propagation impairment mitigation techniques, and satellite communication adaptive systems.



Danielle Vanhoenacker-Janvier received the degree of Electrical Engineer (1978), and the Ph. D. degree in Applied Sciences (1987) from the Université catholique de Louvain (UCLouvain), Belgium. She is Professor since 2000 and Full Professor since 2007. She was head of the Microwave Laboratory (2001-2006) and in charge of the Student Affairs at the Polytechnic School of Louvain (2001-2011). She is Chair of the Doctoral Commission from 2015. Her main activity domain is the study and modelling of atmospheric effects on propagation of radiowaves

above 10 GHz for more than 30 years, with a special interest in the propagation through turbulent troposphere and in the use of Numerical Weather Prediction software for the simulation of atmospheric effects. New applications are foreseen at optical wavelengths. Her group is also involved in the simulation of the Radar Cross Section of airplanes Wake Vortices and the evaluation of the Doppler spectrum. She is also active in microwave circuits design. She has authored more than 120 technical papers and she is co-author of a book. D. Vanhoenacker-Janvier is reviewer for various international conferences, IEEE and IEE journals and acted as expert for the evaluation of research teams in various countries. She is Secretary General of the European Microwave Association.